DOI: 10.1002/chem.200901671

Versatile Photophysical Properties of *meso*-Aryl-Substituted Subporphyrins: Dipolar and Octupolar Charge-Transfer Interactions

Shanmugam Easwaramoorthi,[a] Jae-Yoon Shin,[a] Sung Cho,[a] Pyosang Kim,[a] Yasuhide Inokuma,[b] Eiji Tsurumaki,[b] Atsuhiro Osuka,*[b] and Dongho Kim*[a]

Abstract: Donor–acceptor systems based on subporphyrins with nitro and amino substituents at *meta* and *para* positions of the *meso*-phenyl groups were synthesized and their photophysical properties have been systematically investigated. These molecules show two types of charge-transfer interactions, that is, from center to periphery and periphery to center depending on the peripheral substitution, in which the subporphyrin moiety plays a dual role as both donor and acceptor. Based on the solvent-polarity-dependent photophysical properties, we have shown that the fluorescence emission of *para* isomers originates from the solvatochromic, dipolar, symmetry-broken, and relaxed excited states, whereas the non-solvatochromic fluorescence of *meta* isomers is of the octupolar type with false symmetry breaking. The restricted *meso*-(4-aminophenyl) rotation at low temperature prevents the intramolecular charge-transfer (ICT)-forming process. The two-photon absorption (TPA) cross-section values were determined by photoexcitation at 800 nm in nonpolar toluene and polar acetonitrile solvents to see the effect of ICT on the TPA processes. The large enhancement in the TPA cross-section value of approximately 3200 GM (1 GM = 10^{-50} cm^4 s photon^{-1}) with donor–acceptor substitution has been attributed to the octupolar effect and ICT interactions. A correlation was found between the electron-donating/-withdrawing abilities of the peripheral groups and the TPA cross-section values, that is, *p*-aminophenyl > *m*-aminophenyl > nitrophenyl. The increased stability of octupolar ICT interactions in highly polar solvents enhances the TPA cross-section value by a factor of approximately 2 and 4, respectively, for *p*-amino- and *m*-nitrophenyl-substituted subporphyrins. On the other hand, the stabilization of the symmetry-broken, dipolar ICT state gives rise to a negligible impact on the TPA processes.

Keywords: absorption · charge transfer · donor–acceptor systems · photophysics · porphyrinoids

Introduction

Two-photon absorption (TPA) processes have received increasing attention over the past twenty years. The multitude of applications include spectroscopy,[1] three-dimensional optical storage,[2–6] micro- to nanofabrication,[7–9] and three-dimensional imaging of biological systems.[10–13] As part of the mission of increasing TPA efficiency, molecules showing intramolecular charge-transfer (ICT) interactions between donor (D) and acceptor (A) groups through intervening π-conjugation bridges have been identified to be quite promising.[14–17] For several decades along this line, much attention has been focused on the dipolar molecules, in which the charge asymmetry created by the permanent dipole moment is redistributed under the influence of an intense electromagnetic field through a highly polarizable π-conjugated system, which contributes to the higher nonlinear optical properties of molecules. Recently, attention has turned from these dipolar molecules to branched multipolar molecules such as quadrupolar (D–π-A–π-D or A–π-D–π-A)[18,19] and octupolar systems (AD_3 or DA_3), which show non-monotonically increased TPA properties as compared with the sum of their individual dipolar branches.[20–25] Important parameters that influence the TPA properties in octupolar systems

---

[a] Dr. S. Easwaramoorthi, J.-Y. Shin, Dr. S. Cho, P. Kim,
Prof. Dr. D. Kim
Spectroscopy Laboratory for Functional π-Electronic Systems
and Department of Chemistry
Yonsei University, Seoul 120-749 (Korea)
Fax: (+82) 2-2123-2434
E-mail: dongho@yonsei.ac.kr

[b] Y. Inokuma, E. Tsurumaki, Prof. Dr. A. Osuka
Department of Chemistry, Graduate School of Science
Kyoto University, Sakyo-ku, Kyoto 606-8502 (Japan)
Fax: (+81) 75-753-3970
E-mail: osuka@kuchem.kyoto-u.ac.jp

Supporting information for this article is available on the WWW under http://dx.doi.org/10.1002/chem.200901671.

are the following: 1) a first hyperpolarizability that qualitatively exhibits a linear relationship with the TPA processes, 2) multidimensionality of core-to-periphery or periphery-to-core charge transfer, 3) donor and/or acceptor strengths of constitutional segments, and 4) additional coherent coupling between the branches.[26–30]

Typical examples of octupolar molecular systems are three-dimensional π-conjugated systems such as triphenylbenzene[21,26] and triphenylamine derivatives,[17,20] metal–ligand complexes,[31,32] subporphyrins,[33,34] and subphthalocyanines.[35,36] Among these, subporphyrins and subphthalocyanines deserve particular attention because of their rich π-electron networks that communicate through the triangular cone-shaped structure. Since our inception in 2006, we have been continuously exploring the chemistry of subporphyrins,[37] which includes the large substituent effects of *meso*-aryl substituents and peripheral β substituents on the electronic properties,[38] remarkable ICT interactions, and cation-sensing by fluorescence spectroscopy.[39] Importantly, we have unveiled the progressive increase of TPA cross-section values ($\sigma^{(2)}$) from approximately 80 GM (1 GM = 10^{-50} cm^4 s photon^{-1}) for triphenyl subporphyrin (**1**) to 1340 GM for tris-oligo(1,4-phenyleneethynylene) subporphyrins upon 800 nm photoexcitation, which is essentially originating from the octupolar effect.[33] Further enhancement of the $\sigma^{(2)}$ value to 2800 GM has been attained by attaching six phenylethynyl substituents at β positions.[34] In contrast, porphyrins do not show such enhancement with either donor/acceptor perturbation or elongated π conjugation at the *meso*-phenyl group on account of its negligible electronic communication with the porphyrin core caused by the mutually orthogonal orientation. Nevertheless, larger TPA efficiencies of porphyrins have been achieved by the extended π conjugation through multiporphyrins using different linkages.[40,41]

Inspired by the versatile electronic properties of octupolar subporphyrin molecules, herein we report the synthesis and photophysical and TPA properties of *meta* and *para* isomers of *meso*-aminophenyl- (***m*-NH$_2$** and ***p*-NH$_2$**, respectively) and *meso*-nitrophenyl-substituted subporphyrins (***m*-NO$_2$** and ***p*-NO$_2$**, respectively). Aminophenyl-substituted subporphyrins can be regarded as a three-donor–one-acceptor system (D$_3$A) and nitrophenyl-substituted subporphyrins can be regarded as a one-donor–three-acceptor system (DA$_3$). Systematic investigations on the photophysical properties of these subporphyrins reveal the nature and degree of ICT interactions that can be correlated with the TPA efficiencies.

Results

Synthesis: We have synthesized *meta* and *para* isomers of amino- (***p*-NH$_2$** and ***m*-NH$_2$**, respectively) and nitrophenyl- (***p*-NO$_2$** and ***m*-NO$_2$**, respectively) substituted subporphyrins. *meso*-Nitrophenyl-substituted subporphyrins ***p*-NO$_2$** and ***m*-NO$_2$** were synthesized according to our modified Adler protocol, in which peripheral nitro groups were quantitatively reduced by SnCl$_2$·2H$_2$O in a mixture of aqueous EtOH/HCl to afford ***p*-NH$_2$** and ***m*-NH$_2$**, respectively.

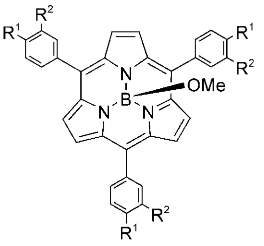

1 $R^1 = R^2 = H$

***p*-NH$_2$** $R^1 = NH_2, R^2 = H$

***m*-NH$_2$** $R^1 = H, R^2 = NH_2$

***p*-NO$_2$** $R^1 = NO_2, R^2 = H$

***m*-NO$_2$** $R^1 = H, R^2 = NO_2$

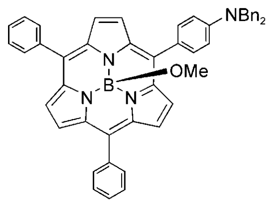

2

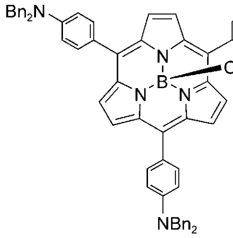

Bn = Benzyl

3

Crystal structure and NMR spectroscopy: A single crystal of ***p*-NH$_2$** suitable for X-ray diffraction analysis was obtained by recrystallization from THF/methanol. The crystallographic data of ***p*-NH$_2$** are summarized in the Experimental Section, and the structure is shown in Figure 1. The crystal lattice includes two independent ***p*-NH$_2$** molecules, in which the dihedral angles of the *meso*-aryl rings with respect to the mean plane of the subporphyrin core are 41.2, 45.4, and 57.9° for one subporphyrin, and 44.1, 48.2, and 58.6° for the other. As seen in *meso*-(*N,N*-dibenzylamino)phenyl subporphyrin **3**,[39] ***p*-NH$_2$** also exhibits considerable bond-length alternation for its all-*meso* 4-aminophenyl rings. The bond lengths between C(1)−C(2), C(3)−C(4), C(4)−C(5), and C(6)−C(1) are in the range from 1.386–1.401, whereas those of C(2)−C(3) and C(5)−C(6) are in the range from 1.376–1.383 Å, thereby indicating a clear quinonoid-type bond alternation. On the other hand, 4-nitrophenyl analogue ***p*-NO$_2$**, as we reported in our previous paper,[38] does not show such distinctive bond-length alternation for its *meso*-aryl rings, although each C−C bond length is slightly different from that of ideal benzene rings. Besides, structural parameters for the subporphyrin cores of ***p*-NH$_2$** and ***p*-NO$_2$** are essentially the same. These results might be indicative of rather stronger interactions between the *meso*-(4-aminophenyl) substituent and the subporphyrin core than those between the 4-nitrophenyl and the core in the ground state.

Although a lot of intermolecular hydrogen bonds, which might change the stable dihedral angles in the solid state, were observed in the structure, such low dihedral angles suggest a low rotational barrier of *meso*-aryl rings and thus strong conjugative interactions between the *meso*-aryl substituents and subporphyrin core. More evidently, the ^{1}H NMR spectrum of ***p*-NH$_2$** shows a couple of doublets at $\delta = 7.86$ and 7.00 ppm due to the *meso*-aryl protons, thereby

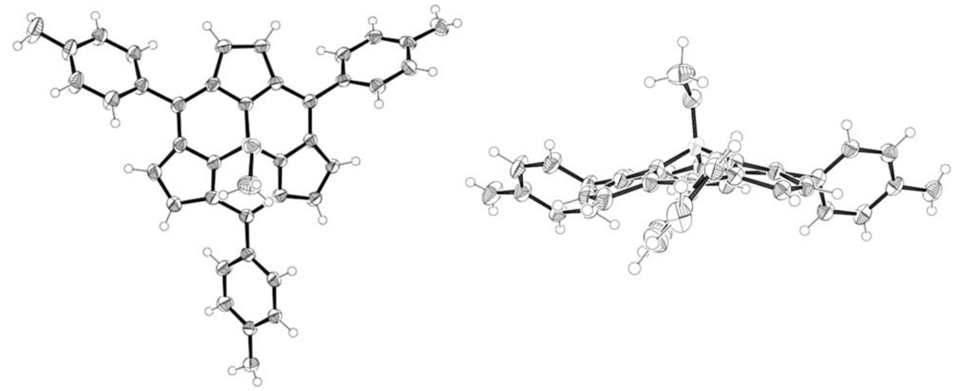

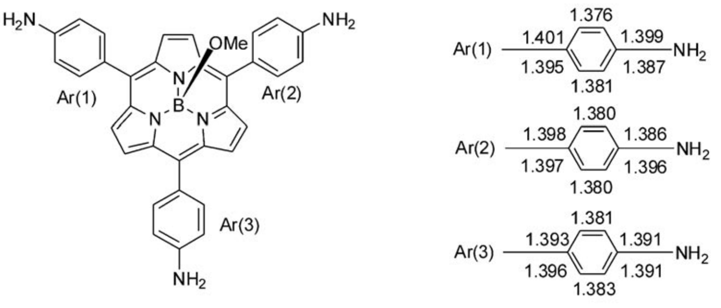

***p*-NH$_2$**

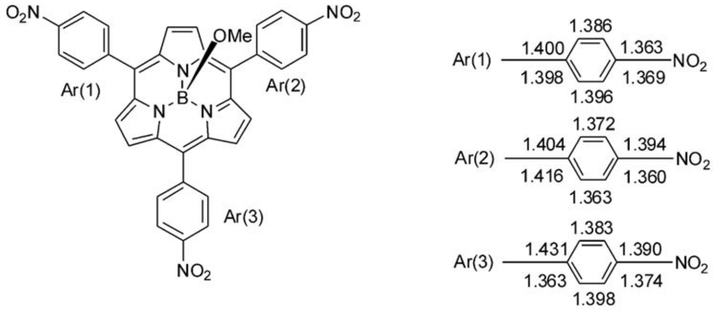

***p*-NO$_2$**

Figure 1. The crystal structure of ***p*-NH$_2$**.

indicating its rapid rotation in solution on the NMR spectroscopic timescale. The solid-state structure of ***p*-NO$_2$** is similar to that of ***p*-NH$_2$**.[38] In addition, the *meta*-substituted subporphyrins ***m*-NH$_2$** and ***m*-NO$_2$** exhibit one singlet each due to the β protons and a single signal set due to the *meta*-substituted phenyl groups at room temperature in CDCl$_3$. These results show that the free rotation of *meso*-aryl groups is also allowed for ***m*-NH$_2$** and ***m*-NO$_2$**, and thus π-conjugative interactions between the *meso*-aryl group and core are significant both for ***m*-NH$_2$** and ***m*-NO$_2$**.

MO calculations: Figure 2 shows the MO diagrams of the subporphyrins **1**, ***p*-NH$_2$**, ***m*-NH$_2$**, ***p*-NO$_2$**, and ***m*-NO$_2$** calculated by using the Gaussian 03 program at the B3LYP/6-31G* level.[42] In the MOs of subporphyrins ***p*-NH$_2$**, the orbital energy levels of both HOMO and LUMO are destabilized due to the electron-donating character of the amino groups.

Importantly, the largest impact of the amino groups is seen in the HOMO(a$_1$) of ***p*-NH$_2$**, in which the orbital coefficients are fully delocalized on both the subporphyrin core and *meso*-aryl substituents; the destabilization energy from the HOMO of **1** was calculated to be 0.60 eV. On the other hand, the destabilization energy of ***m*-NH$_2$** has been estimated to be only 0.22 eV. These results delineate that the substituent effect on *para* positions is significantly larger than that of *meta* positions. The energy difference in the HOMO−1(a$_2$) between ***p*-NH$_2$** and ***m*-NH$_2$** is quite small, which is attributed to ineffective conjugation with *meso* substituents through node points at *meso* positions.

In the cases of ***p*-NO$_2$** and ***m*-NO$_2$**, the frontier orbitals are largely stabilized due to the electron-withdrawing character of the nitro group. Interestingly, the LUMOs of ***p*-NO$_2$** and ***m*-NO$_2$** are spread over the *meso*-attached nitrophenyl moieties. Subporphyrin ***p*-NO$_2$** exhibits the highest stabilization in LUMO energy (ca. 1.1 eV). As a consequence, the HOMO–LUMO gaps were calculated to be 3.18, 2.94, 3.13, 2.94, and 3.16 eV for **1**, ***p*-NH$_2$**, ***m*-NH$_2$**, ***p*-NO$_2$**, and ***m*-NO$_2$**, respectively. It can be concluded that the smallest HOMO–LUMO gaps of 2.94 eV in ***p*-NH$_2$** and ***p*-NO$_2$** are caused by a large electronic interaction at *para* positions, namely, the significant destabilization of the HOMO for ***p*-NH$_2$** or stabilization of the LUMO for ***p*-NO$_2$** by the electron-donating and -withdrawing characters of the amino and nitro groups, respectively.

Steady-state spectral properties: Figure 3 shows the steady-state absorption and fluorescence spectra of **1**, ***p*-NH$_2$**, ***m*-NH$_2$**, ***p*-NO$_2$**, and ***m*-NO$_2$** in toluene. In general, the *para* isomers exhibit redshifted B- and Q-like bands compared with the corresponding *meta* isomers. In fact, both the absorption and fluorescence spectra of the latter ones are almost identi-

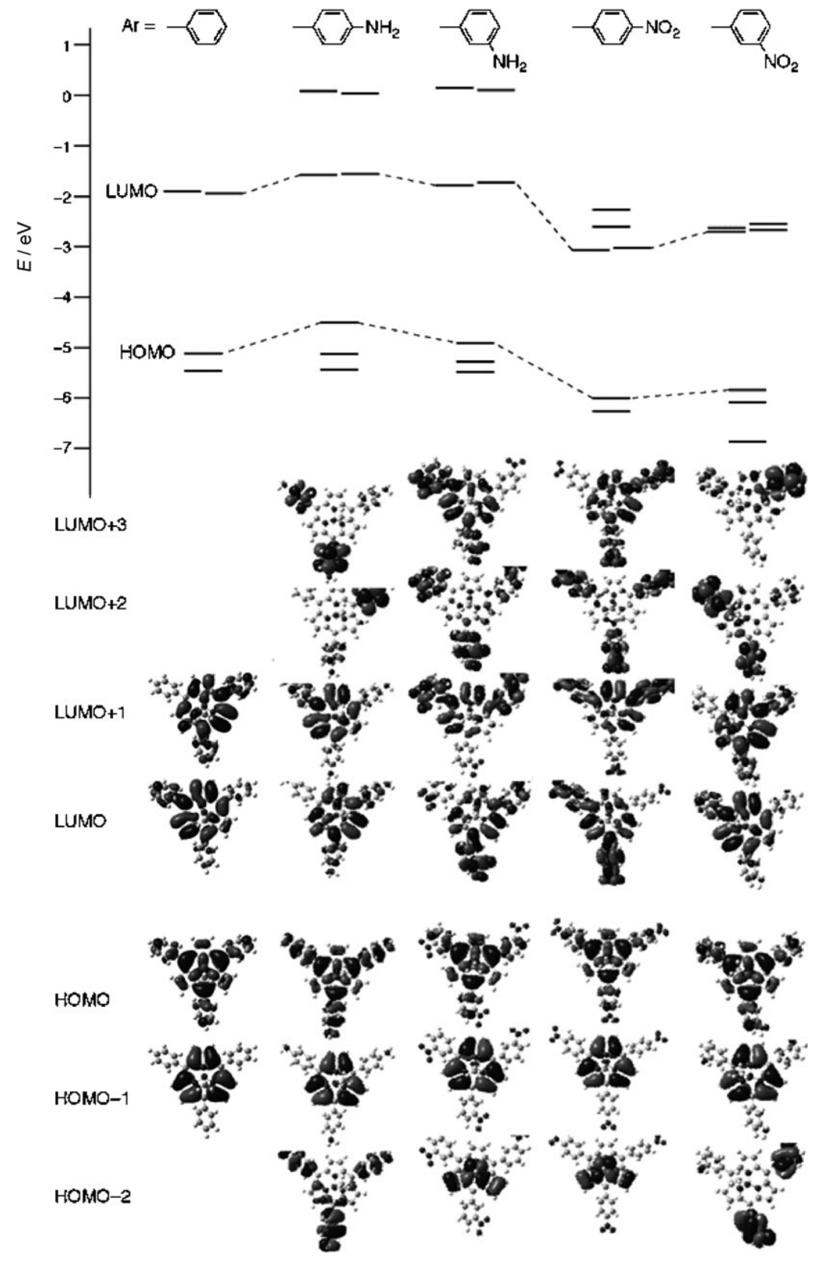

Figure 2. Frontier molecular orbitals (B3LYP/6-31G(d)) of optimized structures of **1**, ***p*-NH$_2$**, ***m*-NH$_2$**, ***p*-NO$_2$**, and ***m*-NO$_2$**.

cal to their parent compound **1**. This feature is ascribed to the inherently weaker influences of *meta* substituents on the electronic property of the subporphyrin core. In addition, the broad single Q-like band of ***p*-NH$_2$** changes into two well-resolved peaks corresponding to Q(1,0) and Q(0,0) transitions in ***m*-NH$_2$**, and the lowest energy Q-band of ***p*-NO$_2$** becomes smeared in ***m*-NO$_2$**. The steady-state fluorescence spectra were observed at 518, 571, 522, 533, and 517 nm for **1**, ***p*-NH$_2$**, ***m*-NH$_2$**, ***p*-NO$_2$**, and ***m*-NO$_2$**, respectively, with the mirror image of their respective Q-bands. The redshifted and intensified fluorescence spectrum of ***p*-NH$_2$** is impressive. In addition, the larger Stokes shifts of 2095 (***p*-NH$_2$**), 1251 (***m*-NH$_2$**), 1481 (***p*-NO$_2$**), and 2256 cm^{-1} (***m*-NO$_2$**) indicate significant structural changes between the ground and excited states. In contrast, the electronic properties of *meso*-aryl-substituted porphyrins remain relatively unperturbed and insensitive to *meta* or *para* substituents due to their nearly orthogonal orientations.

Solvatochromism: Encouraged by the results of our previous investigations on the ICT interactions of *meso*-tris(4-*N*,*N*-benzylaminophenyl)subporphyrin[39] and *meso*-tris(4-nitrophenyl)subporphyrin,[38] we became interested in the structure–property relationship between *meta* and *para* positions and ICT processes. Subporphyrins ***p*-NH$_2$** and ***p*-NO$_2$** exhibit redshifted fluorescence with increased solvent polarity (Figure S1 in the Supporting Information). The quantitative analysis of solvatochromism by the Lippert–Mataga plot[43,44] provided the slopes of 2235 cm^{-1} for ***p*-NH$_2$** and 1061 cm^{-1} for ***p*-NO$_2$**. These large slopes suggest more polar excited states for both subporphyrins but in opposite directions. On the contrary, the absence of such strong solvatochromism for **1**, ***m*-NH$_2$**, and ***m*-NO$_2$** suggests that a change in the excited-state dipole moment induced by the solvent polarity is negligible. The observed small Stokes shifts (≈5 nm) for these compounds are attributed to the refractive index changes of the solvent rather than solvent-polarity-induced dipole moment change. This feature suggests a different operating ICT mechanism (vide infra) for *meta* and *para* isomers.

Fluorescence quantum yields and lifetimes: The fluorescence quantum yields (Φ_f) for subporphyrins in the solvents with different polarities have been determined with reference to Nile red (0.72) in dioxane (Table 1). All the substituted subporphyrin derivatives are more strongly fluorescent in toluene than **1**. For instance, the Φ_f of ***p*-NH$_2$** in toluene is about 57 %, which is approximately four times larger than that of **1** ($\Phi_f = 13\,\%$). The fluorescence quantum yields of all

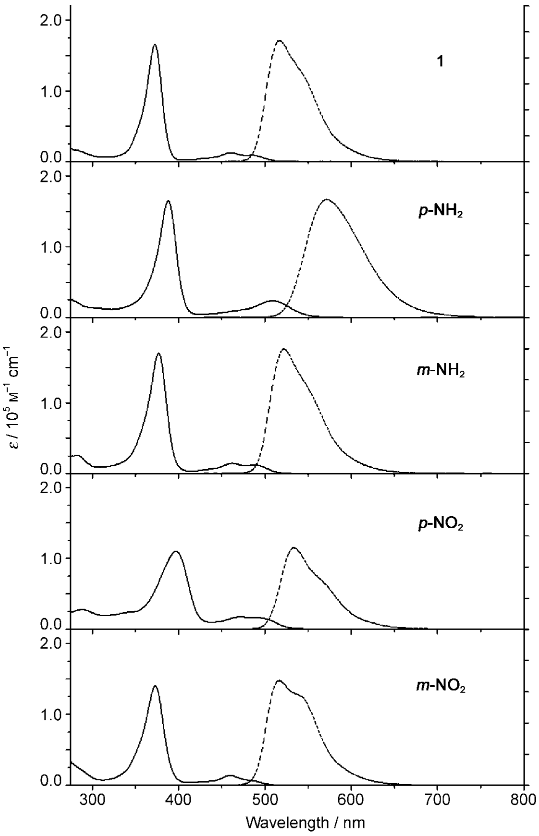

Figure 3. UV/Vis absorption (——) and fluorescence (– – –) spectra of subporphyrins in toluene.

Table 1. Photophysical properties of subporphyrin **p-NH$_2$**, **m-NH$_2$**, **p-NO$_2$** and **m-NO$_2$** in various solvents.

	Solvent	Φ_f[a]	τ_f [ns][b]	k_r [10^8 s^{-1}][c]
p-NH$_2$	toluene	0.57	4.63	1.24
	chloroform	0.46	4.59	1.00
	CH_2Cl_2	0.41	4.88	0.84
	acetone	0.29	4.71	0.62
	CH_3CN	0.26	4.70	0.55
m-NH$_2$	toluene	0.20	2.93	0.68
	chloroform	0.09	2.13	0.42
	CH_2Cl_2	0.09	2.04	0.39
	acetone	0.06	2.14	0.28
	CH_3CN	0.02	1.12	0.16
p-NO$_2$	toluene	0.29	2.80	1.04
	chloroform	0.24	2.20	1.09
	CH_2Cl_2	0.22	1.92	1.15
	acetone	0.20	2.31	0.87
	CH_3CN	0.02	0.18	1.00
m-NO$_2$	toluene	0.27	3.90	0.69
	chloroform	0.05	0.85	0.57
	CH_2Cl_2	0.02	0.39	0.46
	acetone	0.03	0.57	0.52
	CH_3CN	0.005	0.03	1.41

[a] Fluorescence quantum yield. [b] Fluorescence lifetime obtained by the TCSPC method. [c] Radiative rate constant calculated from the fluorescence quantum yield and lifetime (see main text).

donor/acceptor-substituted subporphyrins, however, were found to decrease gradually with an increase in solvent polarity.

The solvent-dependent time-resolved fluorescence decay profiles of **m-NH$_2$** and **m-NO$_2$** are shown in Figure 4 (for **p-NH$_2$**, see Figure S3 in the Supporting Information). The fluorescent decays can be fitted with a single-exponential function and the lifetime (τ_f) values are given in Table 1. Owing to the limitation in the time resolution of our time-correlated single-photon counting (TCSPC) setup ($\approx$100 ps), the fluorescence lifetimes of **p-NO$_2$** and **m-NO$_2$** in acetonitrile were obtained by using a fluorescence up-conversion technique, and the decay profiles are presented in Figure 4c and 4d, respectively. The fluorescence lifetime of **p-NH$_2$**, unlike its Φ_f values, remains insensitive to all the solvents studied here, which has not been observed for other derivatives. Nonetheless, in our recent report we have unveiled solvent-insensitive Φ_f values and fluorescence lifetimes when the amino group is N-substituted with an aryl group.[39] These properties stress the importance of the electron-donor strength or hydrogen-bonding ability for the fluorescence property of **p-NH$_2$**. In contrast, the fluorescence lifetime of the corresponding *meta* derivative **m-NH$_2$** was found to be reduced with increasing solvent polarity (Table 1). On the other hand, the fluorescence lifetime of **m-NO$_2$** (3.9 ns) is longer than **p-NO$_2$** (2.8 ns) in toluene, but in strongly polar acetonitrile that of **m-NO$_2$** becomes considerably shorter (0.03 ns) by a factor of at least four compared to **p-NO$_2$** (0.14 ns) under similar experimental conditions. To obtain a quantitative relationship, the nonradiative (nr) rate constants calculated from the fluorescence quantum yields and lifetimes ($k_{nr}=(1-\Phi_f)/\tau_f$) are plotted against the solvent-polarity parameters $E_T(30)$[45] (Figure S4 in the Supporting Information); **p-NO$_2$** and **m-NO$_2$** are found to show, respectively, 35 and 150 times enhanced nonradiative decay rates in acetonitrile as compared with the nonpolar solvent, toluene, whereas the nonradiative decay rates of **p-NH$_2$** and **m-NH$_2$** are rather insensitive to $E_T(30)$. In the absence of a specific correlation between the nonradiative deactivation rate and the emission energy, the role of internal conversion or intersystem crossing can be neglected in accounting for the faster excited-state deactivation. Notably, despite the absence of solvatochromism in the fluorescence spectra for *meta* isomers, the interesting solvent-dependent fluorescence lifetimes and quantum yields imply the possibility of ICT interactions.

Spectroscopic measurements at low temperatures: Absorption and fluorescence spectra were measured at low temperatures in both a nonpolar toluene/methylcyclohexane (MCH; 1:4) mixture and polar butyronitrile solvents. The absorption spectra were recorded in the temperature range of 173–298 K to explore the influence of free rotation of *meso*-aryl groups on the spectral properties of subporphyrin.[38] Upon lowering the temperature, the absorption spectra of subporphyrin derivatives in the toluene/MCH mixture exhibit substantial changes, which is characteristic of the electron-donating/-withdrawing nature of the substituent and its *para*/*meta* position (Figure S5 in the Supporting Information). For instance, as the temperature was lowered, the B-

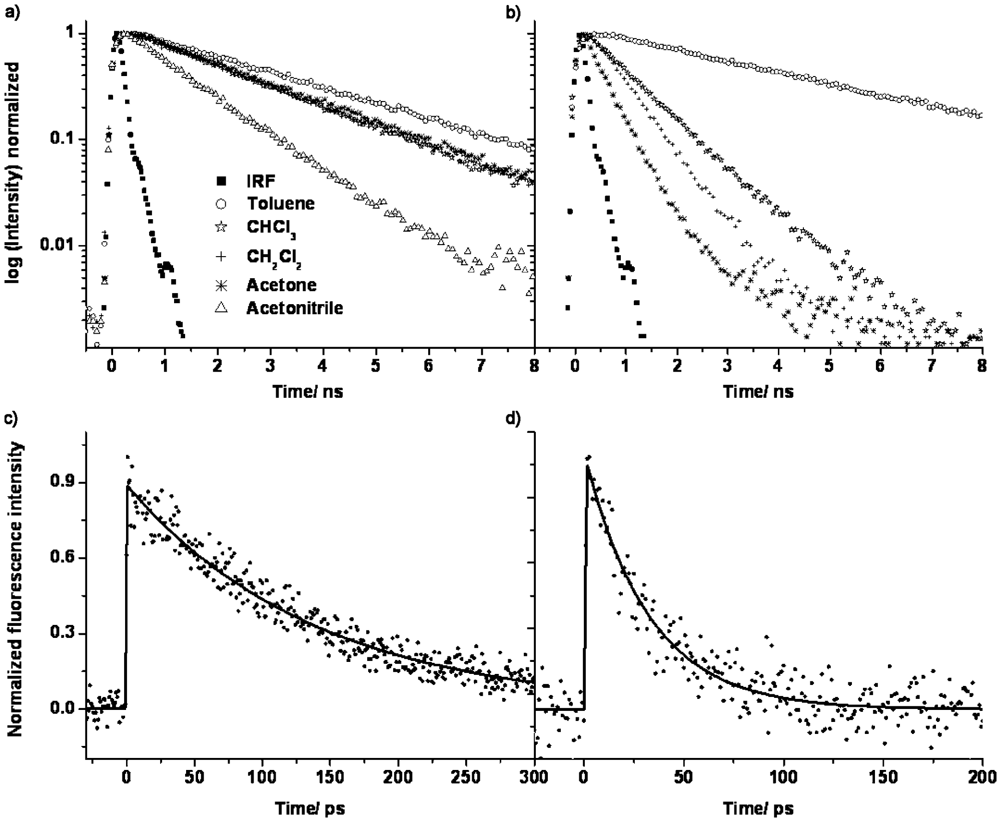

Figure 4. Fluorescence decay profiles of a) ***m*-NH$_2$** and b) ***m*-NO$_2$** in various solvents obtained by the TCSPC method; c) ***p*-NO$_2$** and d) ***m*-NO$_2$** in acetonitrile obtained by the femtosecond fluorescence up-conversion method (the decays are monitored at the respective fluorescence maximum; IRF = instrumental response function).

like bands of **1**, ***p*-NO$_2$**, and ***m*-NO$_2$** were slightly intensified with small redshifts (ca. 2 nm), whereas those of ***p*-NH$_2$** and ***m*-NH$_2$** were broadened with larger redshifts. The temperature dependence of ***p*-NH$_2$** and ***m*-NH$_2$** is similar to that observed for highly conjugated *meso*-alkynyl-substituted multiporphyrins.[46–48] In addition, the notable redshift of the Q-like band for ***p*-NH$_2$** (21 nm) compared with ***m*-NH$_2$** (2 nm) is attributable to the stronger electronic interactions of the *para*-aminophenyl group. Another important parameter is the full width at half-maximum (FWHM) of the absorption bands, which are obviously influenced by the *meso*-aryl group dihedral angle distribution. Accordingly, the differences in FWHM values for B-like bands between 173 and 298 K are −308, 1470, 891, 586, and −235 cm^{-1}, respectively, for **1**, ***p*-NH$_2$**, ***m*-NH$_2$**, ***p*-NO$_2$**, and ***m*-NO$_2$**. The larger FWHM values for ***p*-NH$_2$** and ***m*-NH$_2$** are due mainly to the broad absorption bands at low temperatures, whereas the observed negative FWHM differences for **1** and ***m*-NO$_2$** are caused by the sharper absorption band at low temperatures.

The fluorescence spectra at different temperatures were measured by excitation at three different wavelengths, in which the temperature-change-induced absorption changes were found to be minimal so that the observed trend was independent of the excitation wavelength. As a general trend, a slightly redshifted narrow spectrum was observed upon lowering the temperature, but the changes in the Stokes shift remain fairly small and nearly temperature independent. In addition, the FWHM values of fluorescence spectra were found to be smaller at low temperatures and the differences between the highest (298 K) and lowest (178 K) temperature in a mixture of toluene/MCH were calculated to be 656, 368, 73, 452, and 166 cm^{-1}, respectively, for **1**, ***p*-NH$_2$**, ***m*-NH$_2$**, ***p*-NO$_2$**, and ***m*-NO$_2$**, and a similar trend was also observed for butyronitrile solvent. Figure 5 shows the fluorescence spectra of ***p*-NH$_2$** in a toluene/MCH mixture and butyronitrile at temperatures ranging from 163 to 298 K. Evidently, ***p*-NH$_2$** shows strongly suppressed fluorescence in a toluene/MCH mixture at low temperature, but in contrast, a small increase is noted in butyronitrile. The reference molecule **1**, *meso*-phenyl-substituted analogues ***m*-NH$_2$** (toluene/MCH and butyronitrile), ***p*-NO$_2$** (toluene/MCH), and ***m*-NO$_2$** (butyronitrile) show enhanced fluorescence as the temperature decreases, whereas that of ***p*-NO$_2$** in butyronitrile is nearly intact (Figure S6 in the Supporting Information). A quantitative relationship with temperature can be obtained from the relative fluorescence quantum-yield measurements (corrected for the absorbance changes) in comparison with that at room temperature as a reference.

Consequently, the fluorescence quantum yield of ***p*-NH$_2$** in a toluene/MCH mixture decreases gradually from 57 % at 298 K to 14 % at 193 K and becomes saturated beyond 193 K, but in butyronitrile it remains fairly independent of

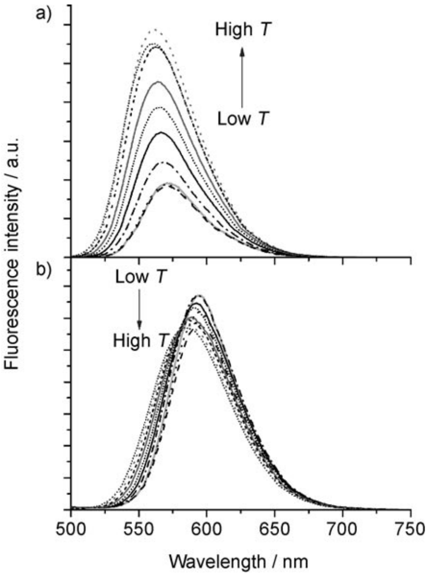

Figure 5. Temperature-dependent fluorescence spectra of **p-NH$_2$** in a) a MCH/toluene mixture and b) butyronitrile in the temperature range from 163 to 298 K at 15 K intervals.

temperature (Figure 6). In contrast, **1**, **m-NH$_2$**, **p-NO$_2$**, and **m-NO$_2$** exhibit nearly temperature-independent fluorescence quantum yields within the experimental error.

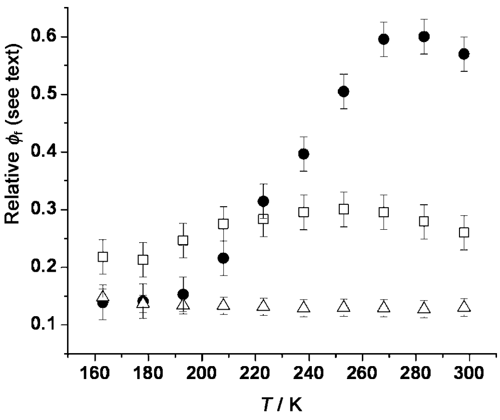

Figure 6. A plot of relative fluorescence quantum yields of **p-NH$_2$** and **1** versus temperature (the maximum possible error limit in fluorescence quantum yields is 10 %): ● **p-NH$_2$** in MCH/toluene; □ **p-NH$_2$** in butyronitrile; △ **1** in MCH/toluene.

Two-photon absorption processes: The TPA cross-section ($\sigma^{(2)}$) values were obtained by using a Z-scan technique[49] by excitation at 800 nm with a femtosecond (≈120 fs FWHM) Ti:sapphire oscillator system. The typical Z-scan traces of **p-NH$_2$** and **m-NO$_2$** are given in the Supporting information (Figures S7–S8) and the $\sigma^{(2)}$ values in toluene and acetonitrile solvents are presented in Table 2. As revealed in Table 2, the $\sigma^{(2)}$ values were found to increase significantly from approximately 80 (**1**) to 360 (**p-NO$_2$**), 850 (**m-NH$_2$**), and 1400 GM (**p-NH$_2$**) in toluene. The $\sigma^{(2)}$ measurements of **m-NO$_2$** were carried out in dichloromethane and a dichloromethane/acetonitrile (1:2) mixture due to the poor solubility in toluene. The determined $\sigma^{(2)}$ values roughly follow the order of **p-NH$_2$** > **m-NH$_2$** > **p-NO$_2$** ≅ **m-NO$_2$**. Notably, **p-NH$_2$** and **m-NH$_2$** exhibit larger TPA values than **p-NO$_2$** and **m-NO$_2$**. As the TPA properties of molecules are influenced by the magnitude of ICT interactions, we have also measured the $\sigma^{(2)}$ values in acetonitrile, in which the ICT state is expected to be considerably more stabilized than that in toluene. Evidently, the $\sigma^{(2)}$ value of **p-NH$_2$** is enhanced significantly from 1400 to 3200 GM in going from toluene to acetonitrile solvent. Similar enhancement of the $\sigma^{(2)}$ value of **m-NO$_2$**, from 400 to 1600 GM, is also observed in going from dichloromethane to dichloromethane/acetonitrile (1:2) mixture. However, those of **m-NH$_2$** and **p-NO$_2$** remain rather constant within the experimental uncertainty.

Table 2. Summary of two-photon absorption cross-section values obtained by 800 nm, 120 fs photoexcitation in different solvents.

Molecule	Solvent	$\sigma^{(2)}$ [GM]	$\Phi\sigma^{(2)}$ [GM]	$\sigma^{(2)}/M_r$ [GM g^{-1} mol^{-1}]	$\Phi\sigma^{(2)}/M_r$ [GM g^{-1} mol^{-1}]
1	CH_2Cl_2	80 ± 30	9	0.16	0.02
p-NH$_2$	toluene	1400 ± 200	798	2.57	1.46
	CH_3CN	3200 ± 300	832	5.87	1.53
m-NH$_2$	toluene	850 ± 100	170	1.56	0.31
	CH_3CN	920 ± 100	18	1.69	0.03
p-NO$_2$	toluene	360 ± 50	104	0.57	0.16
	CH_3CN	450 ± 50	9	0.71	0.01
m-NO$_2$	CH_2Cl_2	400 ± 50	108	0.63	0.17
	CH_2Cl_2/ CH_3CN (1:2)	1600 ± 200	8[a]	2.52	0.01
3	toluene	1900 ± 200	1116	3.02	1.77
	CH_3CN	1800 ± 200	988	2.86	1.57

[a] The Φ_f value in acetonitrile is used.

Discussion

ICT in octupolar molecules: The charge resonance for the linear, dipolar molecule with a donor–acceptor pair can be described by two electronic states,[50] $DA \leftrightarrow D^+A^-$, which have been accompanied by a larger dipole moment change between the ground and excited states, apparently identified by strong fluorescence solvatochromism. On the other hand, multibranched, multipolar systems comprising more than one donor–acceptor group exhibit at least two types of charge-resonance structures that depend upon the cumulative or subchromophoric behaviors of donor–acceptor pairs. Specifically, one of the plausible charge-resonance structures for quadrupolar (ADA or DAD) and octupolar systems (AD_3 or DA_3), respectively, can be denoted as $DAD \leftrightarrow D^{\delta+}A^-D^{\delta+}$ and $DA(D)D \leftrightarrow D^{\delta+}A^-(D^{\delta+})D^{\delta+}$. Because of their highly symmetric structures, the CT has not been accompanied by a significant dipole moment change, and hence, is expected to show non-solvatochromic fluorescence.[51,52] Nonetheless, several examples have been reported in the literature of quadrupolar[53] and octupolar molecules[22,54,55] that exhibit solvatochromic fluorescence similar to dipolar molecules, which is related to the symmetry breaking in the excited state by the formation of a relaxed, dipolar excited state localized on one of the donor–acceptor pairs. The CT states for quadrupolar and octupolar molecules can be described by three $(DAD\leftrightarrow D^{+}A^{-}D\leftrightarrow DA^{-}D^{+})$ and four charge-resonance structures, respectively (Scheme S1 in the Supporting Information).

Despite the octupolar symmetry of subporphyrins, a large Stokes shift of *para* isomer with increasing solvent polarity, reminiscent of that of dipolar chromophores, can be attributed to the excited-state symmetry-breaking through the formation of solvatochromic, dipolar, and a relaxed excited state.[54–58] Thus, the formed CT state can be explained by three charge-resonance structures in which only one *meso*-aryl group takes part in the excited charge-separated state simultaneously (Scheme S1).[59,60] In particular, the longer fluorescence lifetime and higher fluorescence quantum yield of ***p*-NH₂** indicate the formation of an intramolecular-conjugated CT state with a quinonoid-type structure localized on one of the *meso*-aminophenyl groups. The CT state of ***p*-NH₂** is depicted in Scheme 1, which can be regarded as a homologue of boron dipyrromethane (BODIPY) dye.[61]

This consideration has been strongly supported by the facts that the observed solvatochromic behaviors such as fluorescence quantum yield and lifetime and the slope of the Lippert–Mataga plot of ***p*-NH₂** are nearly identical to those of *mono-N,N*-dibenzylaminophenyl-substituted subporphyrin **2**.[39] The radiative rate constant calculated from the fluorescence quantum yield and lifetime using the relationship of $k_r = 1/\tau_0$ and $\tau_0 = \tau_f/\Phi_f$ decreases gradually from 1.24×10^{8} to $0.55\times10^{8}\,s^{-1}$ in going from nonpolar toluene to polar acetonitrile (Table 1). In contrast, the radiative rate remains virtually solvent independent for tris-*N,N*-dibenzylaminophenyl-substituted subporphyrin **3**.[39] As ***p*-NH₂** and **3** show similar ICT interactions, the difference in the radiative rate could arise from the hydrophobic nature and different hydrogen-bonding characters of *N,N*-dibenzylamino groups.[38,39] The symmetry-broken localized ICT state is probably not accessible through relaxation of the Franck–Condon excited state but through an activated rotation process of the *meso*-aryl group, as shown in Figure 7.[51,60] Thus, the fluorescence of ***p*-NH₂** shows high dependence upon the solvent polarity and temperature.

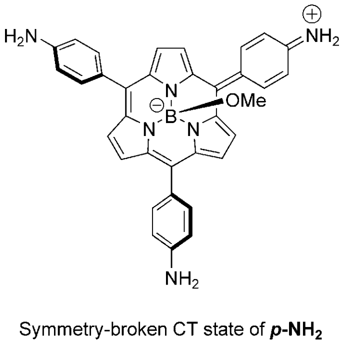

Scheme 1. The symmetry-broken CT state of ***p*-NH₂**.

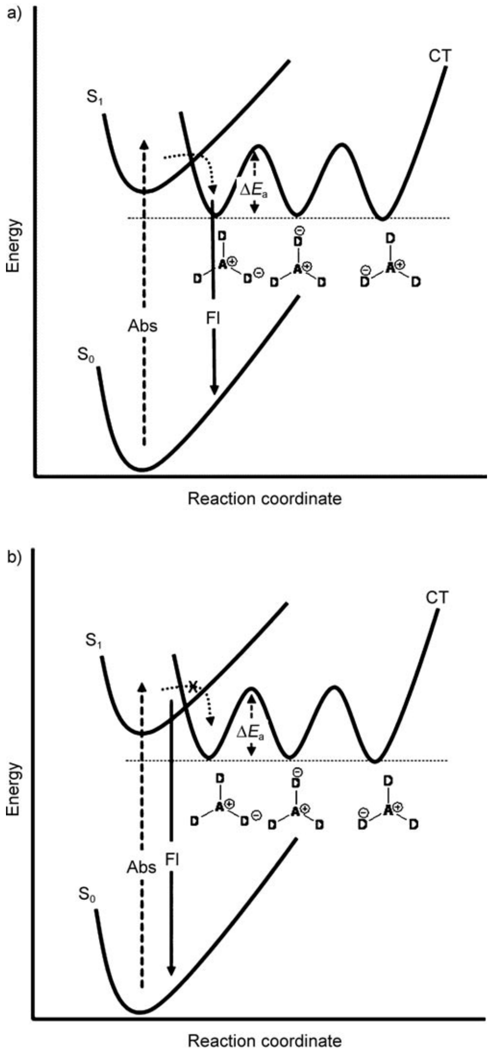

Figure 7. Potential-energy diagram of relative energy levels of charge-resonance structures in nonpolar solvent at a) RT and b) low temperature (Abs = absorption, Fl = fluorescence, E_a = activation energy).

In **3**, the ICT state is thought to be truly localized with the involvement of one *N,N*-dibenzylaminophenyl group, which may explain the observed solvent-insensitive intense fluorescence. Meanwhile, the facile rotation of the unsubstituted aniline groups in ***p*-NH₂** leads to effective charge delocalization between three equivalent, degenerate ICT states as a result of fast interconversion (tunneling) between the resonance structures, thus decreasing the radiative decay rate.[60] Indeed, a similar behavior has been noted previously for multibranched molecules[62] in which those with three side arms show an increased radiative decay rate relative to monomers and dimers due to the delocalization of excitonic states between the branches. On the other hand, ***p*-NO₂** undergoes a photoinduced ICT processes from the subporphyrin core to the *meso*-nitrophenyl substituent. The excited state of ***p*-NO₂** is also expected to be localized on one of the *meso*-nitrophenyl groups and the subporphyrin core, and thus it shows a solvent-polarity-induced Stokes shift. Indeed, a substantial slope in the Lippert–Mataga plot for ***p*-NO$_2$** (1061 cm^{-1}) was observed, which is, however, smaller than that of ***p*-NH$_2$** (2235 cm^{-1}).

Interestingly, the absence of a solvatochromic redshift for ***m*-NH$_2$** and ***m*-NO$_2$** suggests that the ICT interaction is of octupolar nature and therefore, unlike their *para* congeners, is not accompanied by the solvent-induced dipole moment changes. Furthermore, the accelerated nonradiative decay of *meta* isomers in polar solvents ascertains stronger charge-transfer interactions than *para* isomers. In fact, different types of ICT interactions of *ortho*-, *meta*-, and *para*-phenyl-substituent positions[63,64] have been well established for the dipolar molecules with a single donor–acceptor pair. Nevertheless, this is the first report, to the best of our knowledge, that the octupolar molecule exhibits two different types of ICT mechanisms depending on the *meso*-phenyl-substitution position. This result may be interpreted as follows: A restricted *meso*-phenyl rotational motion by *meta*-phenyl substituents (relative to *para*-phenyl substituents) due to the steric hindrance between the substituent and subporphyrin core, which prevents a symmetry-broken, dipolar, ICT-forming process. However, considering the distance between the *meta* substituent and subporphyrin core, the free rotation of the *meso*-phenyl ring is seemingly not affected by the *meta* substituents. In addition, NMR spectroscopic data also confirms the free *meso*-phenyl rotation of *meta* isomers, thus the influence of steric factors on the different ICT interactions can be ruled out. The other possibility would be the appreciable difference in electronic coupling between the *meta* and *para* isomeric forms. As the ICT interactions are driven by through-bond interactions, the direct linkage across *meta* positions is less effective due to their inherently weaker electronic coupling than the linkage across *para* positions. Thus the poor electron delocalization through *meta*-phenyl positions accounts for the unfavorable symmetry-broken, dipolar, ICT-forming process, thereby resulting in non-solvatochromic octupolar ICT interactions.

Temperature-dependent fluorescence: As a unique feature of octupolar donor–acceptor systems, subporphyrins exhibit highly variable optical properties that arise from large electronic interactions between the polar *meso*-aryl substituents and the subporphyrin core. In this context, the rotational freedom of the *meso*-aryl group gains much significance. Thus we have examined the fluorescence spectra at different temperatures to reveal the role of such rotational motions of the *meso*-aryl substituents in the electronic interactions systematically. Explicitly, the larger electronic interactions due to the enhanced coplanarity can be seen from the temperature-dependent absorption spectral changes such as the redshifted B-like absorption bands (Figure S5 in the Supporting Information). Besides, the broad absorption peaks with large FWHM values at low temperatures, except for **1** and ***m*-NO$_2$**, indicate the existence of various conformers with a distribution of dihedral angles between the *meso*-phenyl and the subporphyrin core. But the fluorescence at low temperature arises from the relaxed excited state, as can be seen from the relatively smaller FWHM values of the fluorescence band. Particular attention in this section is paid to ***p*-NH$_2$**, because it shows dramatically decreased fluorescence intensity in a mixture of methylcyclohexane/toluene upon lowering the temperature. Such changes are crucial to gaining information on the charge-transfer mechanism because structural changes are accompanied by intramolecular charge transfer.[65] In this context, the temperature-dependent Φ_f values were examined to elucidate the role of conformational relaxation in the formation of the ICT state as discussed below.

The large Φ_f value of ***p*-NH$_2$** in a mixture of methylcyclohexane/toluene that arises from the localized ICT state has largely been suppressed at low temperatures because of a certain activation barrier. Quite intriguingly, the Φ_f value of ***p*-NH$_2$** at 173 K is equivalent to that of **1**. This feature can be directly correlated to the formation of a dipolar, localized, emissive ICT state that is accessible through *meso*-4-aminophenyl group rotation and not through the Frank–Condon relaxation process. At low temperatures, the molecule in the S_1 state cannot undergo such a process to form a localized ICT state (Figure 7b), since the rotational motion of the *meso*-aminophenyl group is significantly restricted. Thus the fluorescence at low temperatures comes from the Frank–Condon state with low Φ_f. Similar phenomena have commonly been observed for the molecules that show twisted intramolecular charge-transfer (TICT) processes in which the low-energy TICT emission is considerably reduced or vanished at low temperatures due to the frozen conformational relaxation that prevents the formation of the electronically decoupled TICT state.[65] Furthermore, our interpretation is also in a good agreement with the previous reports on the multibranched quadrupolar and octupolar structures for which the symmetry breaking in nonpolar solvent depends on the height of the energy barrier that separates the identical, degenerate charge-resonance structures.[60,66] In this case, the symmetry breaking occurs through the excitonic interaction between the branches; however, in the present subporphyrin case, it occurs through the π-conjugation pathway of the subporphyrin moiety accompanied by *meso*-aryl group rotation. On the contrary, despite enhanced mesomeric interactions upon lowering the temperature, for ***p*-NH$_2$** in polar solvent, butyronitrile, the Φ_f remains nearly constant within the experimental uncertainty. This observation is consistent with our interpretation (vide supra) that the ICT interaction in polar solvent at room temperature is of an octupolar nature due to the facile charge resonance between all the *meso*-*p*-aminophenyl groups (three-dimensional charge transfer) and hence has not been significantly affected by the restricted *meso*-aryl group rotation at low temperatures, which is responsible for the unchanged Φ_{fl} irrespective of temperature, similar to its *meta* congener.

Two-photon absorption processes: The third-order nonlinear optical properties of donor–acceptor-substituted subporphyrin molecules can be accessed from their $\sigma^{(2)}$ values. The drastic enhancement of $\sigma^{(2)}$, from approximately 4 to the maximum of about 32 times, depending on the substituents, can be ascribed to the ICT interactions between donor and acceptor moieties as well as the octupolar effect. The higher TPA efficiencies of subporphyrins originate from the larger first hyperpolarizability due to the octupolar structure that qualitatively possesses a linear relationship with the $\sigma^{(2)}$ values, and both of them increase monotonically with an increase in the donor and acceptor strength of the substituents.[30] A comparison between the π-conjugative fabrication and donor–acceptor substituents at the *meso*-aryl group of the subporphyrin provides further insight into the structure–property relationship, though both of them are found to enhance the TPA efficiency. The *meso*-oligo(1,4-phenyleneethynylene)-substituted subporphyrins[33] exhibit the $\sigma^{(2)}$ value of 1340 GM, but here it has been shown that even higher TPA efficiency is achieved by ***p*-NH₂**, a far simpler subporphyrin. This result is promising when one considers the smaller molecular weight of ***p*-NH₂**, since such views of atom economy or atom efficiency will be more important in actual applications. These results illustrate the advantages of the charge-transfer interaction over the chain-length elongation in octupolar systems on TPA properties.

In contrast to the investigations on the structure–property relationship of TPA processes at the molecular level, the study of solvent effect is still in a rudimentary stage. Importantly, the magnitude of charge-transfer interactions,[15,67] one of the desired requirements for the TPA property, can be largely perturbed by solvent polarity, and such solvent effects are expected to change the $\sigma^{(2)}$ values. However, there have been few theoretical and computational studies to address the solvent effect, and unfortunately the published results indicate a lack of consensus.[66,68–72] A very recent independent experimental study using vinylbenzene[73] and vinylfluorene[74] derivatives reveals that the two-photon transitions do not correlate with the polarity and polarizability of the solvent unlike one-photon transition. Furthermore, Bazan et al.[53] reported that the solvent-dependent $\sigma^{(2)}$ value of distyrylbenzene chromophores is nonmonotonic; the maximum $\sigma^{(2)}$ value was observed in the solvent with intermediate polarity. On the other hand, the TPA cross-section values of octupolar molecules are expected to show little solvent dependence due to a lack of permanent dipole moment. However, theoretical studies indicate the influence of dipolar, quadrupolar, octupolar, and higher-order interactions with solvent.[71]

The solvent-dependence study in the present investigation is aimed at elucidating the ICT effect on the TPA processes. The $\sigma^{(2)}$ values of subporphyrins remain solvent insensitive except for ***p*-NH₂** and ***m*-NO₂**, which, respectively, show approximately two- and fourfold enhancement in going from toluene to acetonitrile and from dichloromethane to a 1:2 mixture of dichloromethane/acetonitrile, respectively. These behaviors substantiate the significant role played by solvents in influencing the degree of ICT interactions. On the other hand, despite the enhanced degree of ICT interactions, the very small or negligible increase in the $\sigma^{(2)}$ value for ***p*-NO₂** and ***m*-NH₂** is probably due to the comparatively smaller ICT interactions. For ***p*-NO₂**, another probable reason would be the stabilization of the symmetry-broken, stabilized, dipolar state in acetonitrile, which can be negated by reduced octupolar contribution, thus leading to the constant $\sigma^{(2)}$ value. On the contrary, the much larger $\sigma^{(2)}$ value of ***p*-NH₂** in acetonitrile could arise from the enhanced charge delocalization in acetonitrile over toluene. To confirm this hypothesis, we have also measured the $\sigma^{(2)}$ value of **3** under similar conditions, which turned out to be (1850 ± 50) GM in both toluene and acetonitrile. This feature has led to our interpretation that increased octupolar ICT interaction and its subsequent stabilization by polar acetonitrile is responsible for the enhanced $\sigma^{(2)}$ value for ***p*-NH₂**, thereby further underscoring the superiority of the octupolar state over the symmetry-broken dipolar ICT state for the enhanced TPA property of octupolar molecules. This result is in good agreement with the previous reports on triphenylamine derivatives in which three-dimensional charge-transfer interactions are responsible for higher $\sigma^{(2)}$ values.[62] In addition, hyper-Rayleigh scattering (HRS) and electric-field-induced second-harmonic generation (EFISH) studies of nitro-substituted subphthalocyanines indicate that the second-order nonlinear optical properties of subphthalocyanines are also sensitive to the dipolar and octupolar contribution, which in fact can further be tailored by the substitution pattern,[75] similar to subporphyrins. However, in contrast with subporphyrins, higher nonlinear optical (NLO) efficiencies of subphthalocyanines originate from the acceptor substituents rather than the donor substituents.[76] Thus, we can conclude that simple fabrications of subporphyrins by the introduction of *meso*-aryl substituents allows for the tailoring of dipolar and octupolar contributions, and subsequently their TPA properties.

We have also calculated the action cross section[17] defined as the product of the fluorescence quantum yield (Φ_f) multiplied by the $\sigma^{(2)}$ values (Table 2). As a consequence of the enhancement of both $\sigma^{(2)}$ and Φ_f values, the amino-substituted subporphyrins ***p*-NH₂** and ***m*-NH₂** exhibit an approximately one-hundredfold increase in the action cross-section values with respect to **1**. Indeed, the enhancement effect is modulated by the strength of the donor group as can be seen from the order of $\sigma^{(2)}\Phi_f$ values $NBn_2 > p\text{-}NH_2 > m\text{-}NH_2$. To compare the different types of octupolar molecules, the $\sigma^{(2)}$/molecular weight ratio and $\sigma^{(2)}\Phi_f$/molecular weight ratio are shown to be the relevant figures of merit (Table 2).[17] In this aspect, ***p*-NH₂** and its N-substituted analogue are one of the most efficient TPA chromophores of similar molecular size; their $\sigma^{(2)}/M_r$ and $\sigma^{(2)}\Phi_f/M_r$ values are 5.87 and 1.53, respectively.[17] Furthermore, in most of the branched systems previously reported, the increased $\sigma^{(2)}$ values with ICT interactions have been accompanied by a decrease in the fluorescence quantum yield and hence these molecules are not useful for applications that utilize two-photon excited fluorescence. These problems are overruled for our molecules, particularly **3**, which shows a higher fluorescence quantum yield irrespective of the surrounding environment. That makes this molecule an ideal candidate for two-photon fluorescence imaging in a heterogeneous biological environment. Given the smaller size of the molecule with its well-connected π network, the easy functionalization at the β and *meso* positions, and higher sensitivity to *meso*-aryl substituents, the TPA properties of subporphyrins are easily tunable by a judicious choice of substituents.

Conclusion

Herein, we present a systematic study on the photophysical and TPA properties of donor–acceptor-substituted octupolar subporphyrins. Solvatochromic photophysical properties demonstrate the ICT interactions between the donor and acceptor groups either from the center to the periphery or vice versa, depending on the electron-withdrawing/-donating nature of the peripheral substituent. Furthermore, the opposite solvatochromic behavior between *para* and *meta* isomers allows us to quantify the emissive excited state of *para* isomers as the localized, dipolar state due to symmetry breaking, whereas that of *meta* congeners is of an octupolar nature that arises from false symmetry breaking. We have also shown that restricted rotation of a *para*-aminophenyl subporphyrin in nonpolar solvents at low temperatures prevents the formation of a localized excited state, thereby leading to the fluorescence from the Frank–Condon state. Finally, the TPA cross-section values of subporphyrins are drastically enhanced with donor/acceptor substituents by means of octupolar as well as ICT interactions. Given the high fluorescence quantum yield and TPA cross-section value, *p*-aminophenyl-substituted subporphyrins like ***p*-NH$_2$** and **3** would be an ideal candidate for two-photon fluorescence imaging. In fact, the stabilization of octupolar ICT states by polar solvents has proved to be effective for TPA enhancement, whereas that of symmetry-broken dipolar excited states has a negligible or very small influence. We believe that the present study will provide a firm basis for understanding the octupolar and dipolar ICT contributions to the third-order nonlinear optical properties and will guide the design of novel molecules with high versatility.

Experimental Section

Synthesis and characterization: All reagents and solvents were of commercial reagent grade and were used without further purification. ^{1}H, ^{11}B, and ^{13}C NMR spectra were recorded using a JEOL delta-600 spectrometer, and chemical shifts were reported as the delta scale in ppm relative to internal standards, $CHCl_3$ ($\delta = 7.26$ ppm for ^{1}H, 77.16 ppm for ^{13}C), and an external standard, $BF_3{\cdot}OEt_2$ in $CDCl_3$ ($\delta = 0.00$ ppm for ^{11}B). ESI-TOF-MS spectra were recorded using a BRUKER DALTONICS micro TOF LC using positive-ion mode.

Methoxo(5,10,15-triphenylsubporphyrinato)boron(III) (**1**) and methoxo(5,10,15-tri(4-nitrophenyl)subporphyrinato)boron(III) (***p*-NO$_2$**) were prepared according to the reported procedure.[38] Methoxo(5,10,15-tri(3-nitrophenyl)subporphyrinato)boron(III) (***m*-NO$_2$**) was also synthesized from pyridine•tri-*N*-pyrrolylborane (2.00 g, 6.94 mmol) and 3-nitrobenzaldehyde (3.10 g, 20.8 mmol) in 1 % yield (41 mg) by following the same procedure. Aminophenyl-substituted subporphyrins ***p*-NH$_2$** and ***m*-NH$_2$** were prepared by reduction of corresponding nitrophenyl-substituted subporphyrins ***p*-NO$_2$** and ***m*-NO$_2$**, respectively.

Subporphyrin ***p*-NO$_2$** or ***m*-NO$_2$** (ca. 10–50 mg) was dissolved in a minimal amount of chloroform, and the solution was diluted with ethanol (15 mL). Next, 1 M aq HCl (15 mL) and $SnCl_2{\cdot}2H_2O$ (20 equiv) were added to the solution. The resulting solution was vigorously stirred at 70 °C for 7 h. After cooling, 1 M aq NaOH was added to make the solution basic and the products were repeatedly extracted with CH_2Cl_2 until the aqueous layer became colorless. The combined organic layer was washed with brine, dried over anhydrous Na_2SO_4, and the solvent was evaporated. The residue was dissolved in methanol (ca. 20 mL) and the solution was heated at reflux for 30 min. After evaporating the solvent, axially methoxo-coordinated product was recrystallized from CH_2Cl_2/hexane to give *meso*-aminophenyl-substituted subporphyrin (***p*-NH$_2$** as a red solid or ***m*-NH$_2$** as an orange solid) quantitatively.

Methoxo[5,10,15-tri(3-nitrophenyl)subporphyrinato]boron(III) (*m*-NO$_2$): ^{1}H NMR (600 MHz, $CDCl_3$): $\delta = 8.85$ (s, 3H; *meso*-Ar-*o*-H), 8.50 (d, $J = 7.4$ Hz, 3H; *meso*-Ar-*o* or *p*-H), 8.43 (d, $J = 7.4$ Hz, 3H; *meso*-Ar-*o* or *p*-H), 8.14 (s, 6H; β-H), 7.92 (t, $J = 7.4$ Hz, 3H; *meso*-Ar-*m*-H), 0.82 ppm (s, 3H; axial-OMe); ^{11}B NMR (193 MHz, $CDCl_3$): $\delta = -15.4$ ppm (s, 1B); ^{13}C NMR (150 MHz, $CDCl_3$): $\delta = 148.6$, 141.4, 138.8, 138.5, 129.9, 127.4, 123.1, 122.7, 118.6, 46.8 ppm (axial-OMe); UV/Vis (in CH_2Cl_2): λ (ε) = 373 (141 000), 460 nm (14 000 $M^{-1}cm^{-1}$); fluorescence (in CH_2Cl_2, $\lambda_{ex} = 373$ nm); $\lambda_{max} = 512$ nm, $\Phi_F = 8 \times 10^{-3}$; HR-ESI TOF-MS (positive mode): *m/z* calcd for $C_{33}H_{18}N_6B_1O_6$: 605.1381 $[M-OMe]^+$; found: 605.1396.

Methoxo[5,10,15-tri(4-aminophenyl)subporphyrinato]boron(III) (*p*-NH$_2$): ^{1}H NMR (600 MHz, $CDCl_3$): $\delta = 8.08$ (s, 6H; β-H), 7.86 (d, $J = 8.7$ Hz, 6H; *meso*-Ar-*o*-H), 7.00 (d, $J = 8.7$ Hz, 6H; *meso*-Ar-*m*-H), 3.94 (brs, 6H; NH_2), 0.81 ppm (s, 3H; axial-OMe); ^{11}B NMR (193 MHz, $CDCl_3$): $\delta = -15.1$ ppm (s, 1B); ^{13}C NMR (150 MHz, $CDCl_3$): $\delta = 146.4$, 140.7, 134.3, 127.8, 122.0, 120.5, 115.4, 46.9 ppm (axial-OMe); UV/Vis (in CH_2Cl_2): λ (ε) = 388 (165 000), 510 nm (23 000 $M^{-1}cm^{-1}$); fluorescence (in CH_2Cl_2, $\lambda_{ex} = 388$ nm); $\lambda_{max} = 580$ nm, $\Phi_F = 0.41$; HR-ESI TOF-MS (positive mode): *m/z* calcd for $C_{33}H_{24}N_6B_1$: 515.2156 $[M-OMe]^+$; found: 515.2154.

Methoxo[5,10,15-tri(3-aminophenyl)subporphyrinato]boron(III) (*m*-NH$_2$): ^{1}H NMR (600 MHz, $CDCl_3$): $\delta = 8.13$ (s, 6H; β-H), 7.45 (t, $J = 7.6$ Hz, 3H; *meso*-Ar-*m*-H), 7.41 (s, 3H; *meso*-Ar-*o*-H), 7.40 (d, $J = 6.4$ Hz, 3H; *meso*-Ar-*o*-H), 6.92 (d, $J = 8.7$ Hz, 3H; *meso*-Ar-*p*-H), 3.92 (brs, 6H; NH_2), 0.81 ppm (s, 3H; axial-OMe); ^{11}B NMR (193 MHz, $CDCl_3$): $\delta = -15.3$ ppm (s, 1B); ^{13}C NMR (150 MHz, $CDCl_3$): $\delta = 146.6$, 140.9, 138.4, 129.5, 123.9, 122.2, 120.7, 120.0, 114.6, 46.8 ppm (axial-OMe); UV/Vis (in CH_2Cl_2): λ (ε) = 377 (170 000), 489 nm (12 000 $M^{-1}cm^{-1}$); fluorescence (in CH_2Cl_2, $\lambda_{ex} = 377$ nm); $\lambda_{max} = 522$ nm, $\Phi_F = 0.09$; HR-ESI TOF-MS (positive mode): *m/z* calcd for $C_{33}H_{24}N_6B_1$: 515.2156 $[M-OMe]^+$; found: 515.2159.

Sample preparation: All the solvents used were of spectroscopic grade (Aldrich) and used without further purification. The fluorescence quantum yields were determined with reference to Nile red in dioxane (0.72) at ambient temperature ((22 ± 1) °C).

Steady-state absorption and fluorescence spectra: Absorption spectra were obtained using a Varian Cary 5000 UV-Vis-NIR spectrophotometer, and steady-state fluorescence spectra were measured using a Hitachi model F-2500/F-4500 fluorometer at room temperature. Temperature-dependent absorption and fluorescence studies were carried out using an Oxford instruments, Optistat DN-V, liquid nitrogen optical spectroscopy cryostat.

Time-correlated single-photon counting: Time-resolved fluorescence was detected using a time-correlated single-photon counting (TCSPC) technique. A homemade cavity-dumped Ti:sapphire oscillator pumped by a CW Nd-YVO4 laser (Coherent, Verdi) was used as the excitation light source; this provided ultrashort pulses (100 fs at FWHM) and allowed for a high repetition rate (ca. 200–400 kHz). The output pulse of the oscillator was frequency-doubled with a second-harmonic crystal. The TCSPC detection system consisted of a multichannel plate photomultiplier (Hamamatsu, R3809U-51) with a cooler (Hamamatsu, C4878), a time-to-amplitude converter (TAC; EG&G Ortec, 457), two discriminators (EG&G Ortec, 584 as signal, and Canberra, 2126 as trigger), and two wide-band amplifiers (Philip Scientific as signal, and Mini Circuit as trigger). A personal computer with a multichannel analyzer (Canberra, PCA3) was used for data storage and processing. The overall instrumental response function (IRF) was about 60 ps (FWHM). A sheet polarizer, set at an angle complementary to the magic angle (54.7°), was placed in the fluorescence collection system. The decay fittings were made by using a least-squares deconvolution fitting process.

Femtosecond time-resolved fluorescence measurements: Femtosecond fluorescence up-conversion apparatus was used for the time-resolved spontaneous fluorescence. The beam source for the S_1 fluorescence was a femtosecond regenerative amplifier consisting of a self-mode-locked femtosecond Ti:sapphire laser (Coherent, MIRA), a Ti:sapphire regenerative amplifier (Clark MXR, CPA-1000) pumped by a Q-switched Nd:YAG laser (ORC-1000), a pulse stretcher/compressor, and an optical detection system. The third harmonic (267 nm) of the fundamental pulses generated by two 100 mm-thick BBO crystals served as the pump pulse. Residual fundamental pulses were used as gate pulses. The pump beam was focused at a 500 mm-thick cuvette containing sample solution by a 5 cm focal length plano-convex lens. The cuvette was mounted on a motor-driven state and moved constantly back and forth across the beam to minimize photodegradation. Collecting the fluorescence and focusing it into a BBO crystal for the frequency conversion was achieved by a reflective microscope objective lens (Coherent). We used two kinds of mixing BBO crystals to improve the signal-to-noise ratio. We measured the S_2 fluorescence by using a 0.5 mm crystal to prevent pulse broadening in the mixing crystal. The FWHM of the cross-correlation functions between the scattered pump pulses and the gate pulses was 300 fs for S_1 fluorescence.

Two-photon absorption cross-section ($\sigma^{(2)}$) measurements: The TPA measurements were performed using the open-aperture Z-scan method with 120 fs pulses at a 5 kHz repetition rate using a Ti:sapphire regenerative amplifier system (Spectra-Physics, Hurricane X). The laser beam was divided into two parts. One was monitored as an intensity reference, and the other was used for the transmittance studies. After passing through a $f = 10$ cm lens, the laser beam was focused to 1 mm quartz cell. As the position of the sample cell was varied along the laser beam direction (z axis), the transmitted laser beam from the sample cell was then probed using a Ge/PN photodiode (New Focus, 2033) as used for reference monitoring. Assuming a Gaussian beam profile, the nonlinear absorption coefficient β can be obtained by curve fitting to the observed open-aperture traces with Equation (1):

$$T(z) = 1 - \frac{\beta I_0 (1 - e^{-\alpha_0 l})}{2\alpha_0 (1 + (z/z_0)^2)} \tag{1}$$

in which α_0 is a linear absorption coefficient, I_0 is the on-axis peak intensity of the incident pulses at the focal point, l is a sample length, and z_0 is the diffraction length of the incident beam. After obtaining the nonlinear absorption coefficient β, the TPA cross section ($\sigma^{(2)}$, in GM units) of a single solute molecule can be determined by using the relationship in Equation (2):

$$\beta = \frac{\sigma^{(2)} N_A d \times 10^{-3}}{h\nu} \tag{2}$$

in which N_A is the Avogadro constant, d is the concentration of the TPA compound in solution, h is the Planck constant, and ν is the frequency of the incident laser beam.

Crystallographic data for *p*-NH$_2$:[77,77] $C_{34}H_{27}BN_6O{\cdot}0.5(C_4H_8O)$; $M_r = 1164.96$; triclinic; $P\bar{1}$; $a = 10.546(4)$, $b = 11.095(4)$, $c = 29.022(7)$ Å; $\alpha = 96.076(10)$, $\beta = 92.018(11)$, $\gamma = 29.022(7)°$; $V = 3136.9(17)$ Å^3; $Z = 4$; $T = 123$ K; $\mu(\mathrm{Mo}_{K\alpha}) = 0.077$ cm^{-1}; 14136 measured reflns; 9926 unique reflns; wR_2 (all data) $= 0.1885$; R_1 ($I > 2\sigma(I)$) $= 0.0598$. The SQUEEZE program in PLATON was used for analysis to remove the disordered solvent densities.[79] CCDC-706701 (***p*-NH$_2$**) contains the supplementary crystallographic data for this paper. These data can be obtained free of charge from The Cambridge Crystallographic Data Centre via www.ccdc.cam.ac.uk/data_request/cif.

Acknowledgements

The work at Yonsei was financially supported by the Star Faculty and World Class University (no. 2008-8-1955) programs of the Ministry of Education, Science and Technology of Korea and the AFSOR/AOARD grant (no. FA4869-08-1-4097). S.E., J.-Y.S, S.C., and P.K. thank the BK21 fellowships. The quantum chemical calculations were performed using the supercomputing resources of the Korea Institute of Science and Technology Information (KISTI). The work at Kyoto was supported by the Grants-in-Aid for Scientific Research Program (A) of MEXT (nos. 19205006 and 20108001 "pi-Space"). Y.I. thanks the JSPS Research Fellowship for Young Scientists.

---

[1] S. Shima, R. P. Ilagan, N. Gillespie, B. J. Sommer, R. G. Hiller, F. P. Sharples, H. A. Frank, R. R. Birge, *J. Phys. Chem. A* **2003**, *107*, 8052–8066.
[2] C. C. Corredor, Z.-L. Huang, K. D. Belfield, *Adv. Mater.* **2006**, *18*, 2910–2914.
[3] E. Ishow, A. Brosseau, G. Clavier, K. Nakatani, R. B. Pansu, J.-J. Vachon, P. Tauc, D. Chauvat, C. R. Mendonca, E. Piovesan, *J. Am. Chem. Soc.* **2007**, *129*, 8970–8971.
[4] D. A. Parthenopoulos, P. M. Rentzepis, *Science* **1989**, *245*, 843–845.
[5] J. H. Strickler, W. W. Webb, *Opt. Lett.* **1991**, *16*, 1780–1782.
[6] S. Kawata, Y. Kawata, *Chem. Rev.* **2000**, *100*, 1777–1788.
[7] W. Zhou, S. M. Kuebler, K. L. Braun, T. Yu, J. K. Cammack, C. K. Ober, J. W. Perry, S. R. Marder, *Science* **2002**, *296*, 1106–1109.
[8] S. Kawata, H.-B. Sun, T. Tanaka, K. Takada, *Nature* **2001**, *412*, 697–698.
[9] B. H. Cumpston, S. P. Ananthavel, S. Barlow, D. L. Dyer, J. E. Ehrlich, L. L. Erskine, A. A. Heikal, S. M. Kuebler, I. Y. S. Lee, D. McCord-Maughon, J. Qin, H. Rockel, M. Rumi, X.-L. Wu, S. R. Marder, J. W. Perry, *Nature* **1999**, *398*, 51–54.
[10] C. Xu, W. Zipfel, J. B. Shear, R. M. Williams, W. W. Webb, *Proc. Natl. Acad. Sci. USA* **1996**, *93*, 10763–10768.
[11] W. Denk, P. B. Detwiler, *Proc. Natl. Acad. Sci. USA* **1999**, *96*, 7035–7040.
[12] D. R. Larson, W. R. Zipfel, R. M. Williams, S. W. Clark, M. P. Bruchez, F. W. Wise, W. W. Webb, *Science* **2003**, *300*, 1434–1436.
[13] W. Denk, J. Strickler, W. W. Webb, *Science* **1990**, *248*, 73–76.
[14] M. Rumi, J. E. Ehrlich, A. A. Heikal, J. W. Perry, S. Barlow, Z. Hu, D. McCord-Maughon, T. C. Parker, H. Rockel, S. Thayumanavan, S. R. Marder, D. Beljonne, J.-L. Bredas, *J. Am. Chem. Soc.* **2000**, *122*, 9500–9510.
[15] M. Albota, D. Beljonne, J.-L. Bredas, J. E. Ehrlich, J.-Y. Fu, A. A. Heikal, S. E. Hess, T. Kogej, M. D. Levin, S. R. Marder, D. McCord-Maughon, J. W. Perry, H. Rockel, M. Rumi, G. Subramaniam, W. W. Webb, X.-L. Wu, C. Xu, *Science* **1998**, *281*, 1653–1656.
[16] G. S. He, L.-S. Tan, Q. Zheng, P. N. Prasad, *Chem. Rev.* **2008**, *108*, 1245–1330.
[17] H. M. Kim, B. R. Cho, *Chem. Commun.* **2009**, 153–164.
[18] E. Zojer, D. Beljonne, P. Pacher, J-L. Brédas, *Chem. Eur. J.* **2004**, *10*, 2668–2680.
[19] E. Zojer, D. Beljonne, T. Kogej, H. Vogel, S. R. Marder, J. W. Perry, J.-L. Bredas, *J. Chem. Phys.* **2002**, *116*, 3646–3658.
[20] F. Terenziani, C. L. Droumaguet, C. Katan, O. Mongin, M. Blanchard-Desce, *ChemPhysChem* **2007**, *8*, 723–734.
[21] J. Brunel, O. Mongin, A. Jutand, I. Ledoux, J. Zyss, M. Blanchard-Desce, *Chem. Mater.* **2003**, *15*, 4139–4148.
[22] C. Katan, F. Terenziani, O. Mongin, M. H. V. Werts, L. Porres, T. Pons, J. Mertz, S. Tretiak, M. Blanchard-Desce, *J. Phys. Chem. A* **2005**, *109*, 3024–3037.

[23] W. W. D. Beljonne, E. Zojer, Z. Shuai, H. Vogel, S. J. K. Pond, J. W. Perry, S. R. Marder, J.-L. Brédas, *Adv. Funct. Mater.* **2002**, *12*, 631–641.

[24] O. Varnavski, A. Leanov, L. Liu, J. Takacs, T. Goodson, *J. Phys. Chem. B* **2000**, *104*, 179–188.

[25] M. A. Oar, J. M. Serin, W. R. Dichtel, J. M. J. Frechet, T. Y. Ohulchanskyy, P. N. Prasad, *Chem. Mater.* **2005**, *17*, 2267–2275.

[26] Y.-K. Lee, S.-J. Jeon, M. Cho, *J. Am. Chem. Soc.* **1998**, *120*, 10921–10927.

[27] S. H. Lee, J. R. Park, M.-Y. Jeong, H. M. Kim, S. Li, J. Song, S. Ham, S.-J. Jeon, B. R. Cho, *ChemPhysChem* **2006**, *7*, 206–212.

[28] A. M. McDonagh, M. G. Humphrey, M. Samoc, B. Luther-Davies, S. Houbrechts, T. Wada, H. Sasabe, A. Persoons, *J. Am. Chem. Soc.* **1999**, *121*, 1405–1406.

[29] K. Sénéchal, O. Maury, H. Le Bozec, I. Ledoux, J. Zyss, *J. Am. Chem. Soc.* **2002**, *124*, 4560–4561.

[30] B. R. Cho, S. B. Park, S. J. Lee, K. H. Son, S. H. Lee, M.-J. Lee, J. Yoo, Y. K. Lee, G. J. Lee, T. I. Kang, M. Cho, S.-J. Jeon, *J. Am. Chem. Soc.* **2001**, *123*, 6421–6422.

[31] H. Le Bozec, T. Renouard, *Eur. J. Inorg. Chem.* **2000**, 229–239.

[32] O. Maury, H. L. Bozec, *Acc. Chem. Res.* **2005**, *38*, 691–704.

[33] Y. Inokuma, S. Easwaramoorthi, S. Y. Jang, K. S. Kim, D. Kim, A. Osuka, *Angew. Chem.* **2008**, *120*, 4918–4921; *Angew. Chem. Int. Ed.* **2008**, *47*, 4840–4843.

[34] E. Tsurumaki, Y. Inokuma, S. Easwaramoorthi, J. M. Lim, D. Kim, A. Osuka, *Chem. Eur. J.* **2009**, *15*, 237–247.

[35] C. G. Claessens, D. Gonzalez-Rodriguez, T. Torres, *Chem. Rev.* **2002**, *102*, 835–854.

[36] G. de La Torre, P. Vazquez, F. Agullo-Lopez, T. Torres, *Chem. Rev.* **2004**, *104*, 3723–3750.

[37] Y. Inokuma, J. H. Kwon, T. K. Ahn, M.-C. Yoo, D. Kim, A. Osuka, *Angew. Chem.* **2006**, *118*, 975–978; *Angew. Chem. Int. Ed.* **2006**, *45*, 961–964.

[38] Y. Inokuma, Z. S. Yoon, D. Kim, A. Osuka, *J. Am. Chem. Soc.* **2007**, *129*, 4747–4761.

[39] Y. Inokuma, S. Easwaramoorthi, Z. S. Yoon, D. Kim, A. Osuka, *J. Am. Chem. Soc.* **2008**, *130*, 12234–12235.

[40] K. S. Kim, J. M. Lim, A. Osuka, D. Kim, *J. Photochem. Photobiol. C* **2008**, *9*, 13–28.

[41] M. O. Senge, M. Fazekas, E. G. A. Notaras, W. J. Blau, M. Zawadzka, O. B. Locos, E. M. Ni Mhuircheartaigh, *Adv. Mater.* **2007**, *19*, 2737–2774.

[42] Gaussian 03, Revision C.02, M. J. Frisch, G. W. Trucks, H. B. Schlegel, G. E. Scuseria, M. A. Robb, J. R. Cheeseman, J. A. Montgomery, Jr., T. Vreven, K. N. Kudin, J. C. Burant, J. M. Millam, S. S. Iyengar, J. Tomasi, V. Barone, B. Mennucci, M. Cossi, G. Scalmani, N. Rega, G. A. Petersson, H. Nakatsuji, M. Hada, M. Ehara, K. Toyota, R. Fukuda, J. Hasegawa, M. Ishida, T. Nakajima, Y. Honda, O. Kitao, H. Nakai, M. Klene, X. Li, J. E. Knox, H. P. Hratchian, J. B. Cross, V. Bakken, C. Adamo, J. Jaramillo, R. Gomperts, R. E. Stratmann, O. Yazyev, A. J. Austin, R. Cammi, C. Pomelli, J. W. Ochterski, P. Y. Ayala, K. Morokuma, G. A. Voth, P. Salvador, J. J. Dannenberg, V. G. Zakrzewski, S. Dapprich, A. D. Daniels, M. C. Strain, O. Farkas, D. K. Malick, A. D. Rabuck, K. Raghavachari, J. B. Foresman, J. V. Ortiz, Q. Cui, A. G. Baboul, S. Clifford, J. Cioslowski, B. B. Stefanov, G. Liu, A. Liashenko, P. Piskorz, I. Komaromi, R. L. Martin, D. J. Fox, T. Keith, M. A. Al-Laham, C. Y. Peng, A. Nanayakkara, M. Challacombe, P. M. W. Gill, B. Johnson, W. Chen, M. W. Wong, C. Gonzalez, J. A. Pople, Gaussian, Inc., Pittsburg, PA, **2003**.

[43] E. Lippert, *Z. Naturforsch. A* **1955**, *10*, 541.

[44] N. Mataga, Y. Kaifu, M. Koizumi, *Bull.Chem. Soc. Jpn.* **1955**, *28*, 690.

[45] C. Reichardt, *Chem. Rev.* **1994**, *94*, 2319–2358.

[46] V. Lin, S. DiMagno, M. Therien, *Science* **1994**, *264*, 1105–1111.

[47] H. L. Anderson, *Inorg. Chem.* **1994**, *33*, 972–981.

[48] S. Easwaramoorthi, S. Y. Jang, Z. S. Yoon, J. M. Lim, C.-W. Lee, C.-L. Mai, Y.-C. Liu, C.-Y. Yeh, J. Vura-Weis, M. R. Wasielewski, D. Kim, *J. Phys. Chem. A* **2008**, *112*, 6563–6570.

[49] M. Sheik-Bahae, A. A. Said, T. H. Wei, D. J. Hagan, E. W. Van Stryland, *IEEE J. Quantum Electron.* **1990**, *26*, 760–769.

[50] S. R. Marder, D. N. Beratan, L. T. Cheng, *Science* **1991**, *252*, 103–106.

[51] F. Terenziani, A. Painelli, C. Katan, M. Charlot, M. Blanchard-Desce, *J. Am. Chem. Soc.* **2006**, *128*, 15742–15755.

[52] M.-S. Yuan, Q. Fang, Z.-Q. Liu, J.-P. Guo, H.-Y. Chen, W.-T. Yu, G. Xue, D.-S. Liu, *J. Org. Chem.* **2006**, *71*, 7858–7861.

[53] H. Y. Woo, B. Liu, B. Kohler, D. Korystov, A. Mikhailovsky, G. C. Bazan, *J. Am. Chem. Soc.* **2005**, *127*, 14721–14729.

[54] C. Le Droumaguet, O. Mongin, M. H. V. Werts, M. Blanchard-Desce, *Chem. Commun.* **2005**, 2802–2804.

[55] F. Terenziani, C. L. Droumaguet, C. Katan, O. Mongin, M. Blanchard-Desce, *ChemPhysChem* **2007**, *8*, 723–734.

[56] C. Katan, F. Terenziani, O. Mongin, M. H. V. Werts, L. Porres, T. Pons, J. Mertz, S. Tretiak, M. Blanchard-Desce, *J. Phys. Chem. A* **2005**, *109*, 3024–3037.

[57] W. Verbouwe, L. Viaene, M. Van der Auweraer, F. C. De Schryver, H. Masuhara, R. Pansu, J. Faure, *J. Phys. Chem. A* **1997**, *101*, 8157–8165.

[58] R. Stahl, C. Lambert, C. Kaiser, R. Wortmann, R. Jakober, *Chem. Eur. J.* **2006**, *12*, 2358–2370.

[59] C. Sissa, F. Terenziani, A. Painelli, *J. Phys. Chem. A* **2008**, *112*, 8697–8705.

[60] F. Terenziani, C. Sissa, A. Painelli, *J. Phys. Chem. B* **2008**, *112*, 5079–5087.

[61] M. Kollmannsberger, K. Rurack, U. Resch-Genger, J. Daub, *J. Phys. Chem. A* **1998**, *102*, 10211–10220.

[62] Y. Wang, G. S. He, P. N. Prasad, T. Goodson, *J. Am. Chem. Soc.* **2005**, *127*, 10128–10129.

[63] S. Murali, W. Rettig, *J. Phys. Chem. A* **2006**, *110*, 28–37.

[64] F. D. Lewis, J.-S. Yang, *J. Am. Chem. Soc.* **1997**, *119*, 3834–3835.

[65] Z. R. Grabowski, K. Rotkiewicz, W. Rettig, *Chem. Rev.* **2003**, *103*, 3899–4032.

[66] F. Terenziani, A. Painelli, C. Katan, M. Charlot, M. Blanchard-Desce, *J. Am. Chem. Soc.* **2006**, *128*, 15742–15755.

[67] F. Terenziani, C. Katan, E. Badaeva, S. Tretiak, M. Blanchard-Desce, *Adv. Mater.* **2008**, *20*, 4641–4678.

[68] C.-K. Wang, K. Zhao, Y. Su, Y. Ren, X. Zhao, Y. Luo, *J. Chem. Phys.* **2003**, *119*, 1208–1213.

[69] K. Zhao, L. Ferrighi, L. Frediani, C.-K. Wang, Y. Luo, *J. Chem. Phys.* **2007**, *126*, 204509.

[70] M. J. Paterson, J. Kongsted, O. Christiansen, K. V. Mikkelsen, C. B. Nielsen, *J. Chem. Phys.* **2006**, *125*, 184501.

[71] P. C. Ray, J. Leszczynski, *J. Phys. Chem. A* **2005**, *109*, 6689–6696.

[72] Y. Luo, P. Norman, P. Macak, H. Agren, *J. Phys. Chem. A* **2000**, *104*, 4718–4722.

[73] M. Johnsen, P. R. Ogilby, *J. Phys. Chem. A* **2008**, *112*, 7831–7839.

[74] I. Fitilis, M. Fakis, I. Polyzos, V. Giannetas, P. Persephonis, J. Mikroyannidis, *J. Phys. Chem. A* **2008**, *112*, 4742–4748.

[75] C. G. Claessens, D. González-Rodríguez, T. Torres, G. Martín, F. Agulló-López, I. Ledoux, J. Zyss, V. R. Ferro, J. M. García de La Vega, *J. Phys. Chem. B* **2005**, *109*, 3800–3806.

[76] B. del Rey, U. Keller, T. Torres, G. Rojo, F. Agulló-López, S. Nonell, C. Martí, S. Brasselet, I. Ledoux, J. Zyss, *J. Am. Chem. Soc.* **1998**, *120*, 12808–12817.

[77] P. van d. Sluis, A. L. Spek, *Acta Crystallogr. Sect. A* **1990**, *46*, 194–201.

[78] A. L. Spek, *Acta Crystallogr. Sec. A* **1990**, c34.

[79] PLATON, A Multipurpose Christallographic Tool, Utrecht Univerity, Utrecht, **2005**.

Received: June 18, 2009